

1 **MULTIWAVELENGTH OBSERVATIONS OF THE AGN 1ES 0414+009**
2 **WITH VERITAS, *Fermi*-LAT, *Swift*-XRT, AND MDM**

3 E. Aliu¹, S. Archambault², T. Arlen³, T. Aune⁴, M. Beilicke⁵, W. Benbow⁶, M. Böttcher⁷,
4 A. Bouvier⁴, V. Bugaev⁵, A. Cannon⁸, A. Cesarini⁹, L. Ciupik¹⁰, E. Collins-Hughes⁸,
5 M. P. Connolly⁹, W. Cui¹¹, R. Dickherber⁵, J. Dumm¹², M. Errando¹, A. Falcone¹³,
6 S. Federici^{14,15}, Q. Feng¹¹, J. P. Finley¹¹, G. Finnegan¹⁶, L. Fortson¹², A. Furniss⁴, N. Galante⁶,
7 D. Gall¹⁷, S. Godambe¹⁶, S. Griffin², J. Grube¹⁰, G. Gyuk¹⁰, D. Hanna², H. Huan¹⁸,
8 G. Hughes¹⁴, C. M. Hui¹⁶, A. Imran¹⁹, O. Jamil⁷, P. Kaaret¹⁷, N. Karlsson¹², M. Kertzman²⁰,
9 J. Kerr⁷, Y. Khassen⁸, D. Kieda¹⁶, H. Krawczynski⁵, F. Krennrich¹⁹, M. J. Lang⁹, K. Lee⁵,
10 A. S. Madhavan¹⁹, P. Majumdar³, S. McArthur⁵, A. McCann², P. Moriarty²¹, R. Mukherjee¹,
11 T. Nelson¹², A. O’Faoláin de Bhróithe⁸, R. A. Ong³, M. Orr¹⁹, A. N. Otte²², N. Park¹⁸,
12 J. S. Perkins^{23,24}, A. Pichel²⁵, M. Pohl^{26,14}, J. Quinn⁸, K. Ragan², P. T. Reynolds²⁷, E. Roache⁶,
13 J. Ruppel^{26,14}, D. B. Saxon²⁸, M. Schroedter⁶, G. H. Sembroski¹¹, G. D. Şentürk²⁹,
14 A. W. Smith^{16,*}, D. Staszak², M. Stroh¹⁷, I. Telezhinsky^{26,14}, G. Tešić², M. Theiling¹¹,
15 S. Thibadeau⁵, K. Tsurusaki¹⁷, A. Varlotta¹¹, V. V. Vassiliev³, M. Vivier²⁸, S. P. Wakely¹⁸,
16 J. E. Ward⁵, A. Weinstein¹⁹, R. Welsing¹⁴, D. A. Williams⁴, B. Zitzer³⁰

*Corresponding Author: aw.smith@utah.edu

¹Department of Physics and Astronomy, Barnard College, Columbia University, NY 10027, USA

²Physics Department, McGill University, Montreal, QC H3A 2T8, Canada

³Department of Physics and Astronomy, University of California, Los Angeles, CA 90095, USA

⁴Santa Cruz Institute for Particle Physics and Department of Physics, University of California, Santa Cruz, CA 95064, USA

⁵Department of Physics, Washington University, St. Louis, MO 63130, USA

⁶Fred Lawrence Whipple Observatory, Harvard-Smithsonian Center for Astrophysics, Amado, AZ 85645, USA

⁷Astrophysical Institute, Department of Physics and Astronomy, Ohio University, Athens, OH 45701

⁸School of Physics, University College Dublin, Belfield, Dublin 4, Ireland

⁹School of Physics, National University of Ireland Galway, University Road, Galway, Ireland

¹⁰Astronomy Department, Adler Planetarium and Astronomy Museum, Chicago, IL 60605, USA

¹¹Department of Physics, Purdue University, West Lafayette, IN 47907, USA

¹²School of Physics and Astronomy, University of Minnesota, Minneapolis, MN 55455, USA

¹³Department of Astronomy and Astrophysics, 525 Davey Lab, Pennsylvania State University, University Park, PA 16802, USA

¹⁴DESY, Platanenallee 6, 15738 Zeuthen, Germany

¹⁵Institut für Physik und Astronomie, Universität Potsdam, 14476 Potsdam-Golm, Germany; DESY, Platanenallee 6, 15738 Zeuthen, Germany

¹⁶Department of Physics and Astronomy, University of Utah, Salt Lake City, UT 84112, USA

¹⁷Department of Physics and Astronomy, University of Iowa, Van Allen Hall, Iowa City, IA 52242, USA

¹⁸Enrico Fermi Institute, University of Chicago, Chicago, IL 60637, USA

¹⁹Department of Physics and Astronomy, Iowa State University, Ames, IA 50011, USA

²⁰Department of Physics and Astronomy, DePauw University, Greencastle, IN 46135-0037, USA

²¹Department of Life and Physical Sciences, Galway-Mayo Institute of Technology, Dublin Road, Galway, Ireland

²²School of Physics & Center for Relativistic Astrophysics, Georgia Institute of Technology, 837 State Street NW, Atlanta, GA 30332-0430

²³CRESST and Astroparticle Physics Laboratory NASA/GSFC, Greenbelt, MD 20771, USA.

²⁴University of Maryland, Baltimore County, 1000 Hilltop Circle, Baltimore, MD 21250, USA.

²⁵Instituto de Astronomia y Física del Espacio, Casilla de Correo 67 - Sucursal 28, (C1428ZAA) Ciudad Autónoma de Buenos Aires, Argentina

²⁶Institut für Physik und Astronomie, Universität Potsdam, 14476 Potsdam-Golm, Germany

²⁷Department of Applied Physics and Instrumentation, Cork Institute of Technology, Bishopstown, Cork, Ireland

²⁸Department of Physics and Astronomy and the Bartol Research Institute, University of Delaware, Newark, DE

ABSTRACT

We present observations of the BL Lac object 1ES 0414+009 in the >200 GeV gamma-ray band by the VERITAS array of Cherenkov telescopes. 1ES 0414+009 was observed by VERITAS between January 2008 and February 2011, resulting in 56.2 hours of good quality pointed observations. These observations resulted in a detection of 822 events from the source corresponding to a statistical significance of 6.4 standard deviations (6.4σ) above the background. The source flux, showing no evidence for variability, is measured as $(5.2 \pm 1.1_{stat} \pm 2.6_{sys}) \times 10^{-12}$ photons $\text{cm}^{-2} \text{s}^{-1}$ above 200 GeV, equivalent to approximately 2% of the Crab Nebula flux above this energy. The differential photon spectrum from 230 GeV to 850 GeV is well fit by a power law with an photon index of $\Gamma = 3.4 \pm 0.5_{stat} \pm 0.3_{sys}$ and a flux normalization of $(1.6 \pm 0.3_{stat} \pm 0.8_{sys}) \times 10^{-11}$ photons $\text{cm}^{-2} \text{s}^{-1}$ at 300 GeV. We also present multiwavelength results taken in the optical (MDM), X-ray (*Swift*-XRT), and GeV (*Fermi*-LAT) bands and use these results to construct a broadband spectral energy distribution (SED). Modeling of this SED indicates that homogenous one-zone leptonic scenarios are not adequate to describe emission from the system, with a lepto-hadronic model providing a better fit to the data.

Subject headings: BL Lacertae objects: individual (1ES 0414 +009, VER J0416+011),
Gamma rays: galaxies

1. Introduction

Among the more substantial accomplishments of the latest generation of imaging atmospheric Cherenkov telescopes (IACTs) is the reliable detection of increasingly distant active galactic nuclei (AGN). While the previous generation of ground based gamma-ray experiments such as the Whipple 10 meter telescope and HEGRA detected comparatively close AGN, the furthest being H 1426+428 at a redshift of 0.129 (Horan et al. 2002), observations with VERITAS, HESS, and MAGIC have shown that it is possible to detect sources of very high energy (VHE) gamma rays (>100 GeV) as far out as redshifts of $z = 0.54$ (Albert et al. 2008a).

The AGN 1ES 0414+009 is among the furthest detected TeV BL Lacertae objects, having a well measured redshift of $z = 0.287$ (Halpern et al. 1991). 1ES 0414+009 was first discovered in an X-ray survey performed by the HEAO 1 A-1 instrument (Ulmer et al. 1980) and was originally associated with a cluster of galaxies. Further radio, X-ray and optical observations led to the association

19716, USA

²⁹Physics Department, Columbia University, New York, NY 10027, USA

³⁰Argonne National Laboratory, 9700 S. Cass Avenue, Argonne, IL 60439, USA

33 of the X-ray source with an X-ray bright BL Lacertae object (Ulmer et al. 1983). Additional X-
 34 ray observations (Wolter et al. 1998; Beckmann et al. 2002) show 1ES 0414+009 to have typical
 35 spectral characteristics of “high frequency peaked BL Lacertae” (HBL) objects, as well as being
 36 comparatively bright in the 2-10 keV band with a luminosity comparable to Markarian 421 and
 37 PKS 2155-304, allowing the possibility that 1ES 0414+009 may be a high-redshift analog of these
 38 well studied TeV blazars.

39 1ES 0414+009 also appears in the *Fermi*-LAT 2-year source catalog, associated with the source
 40 2FGL J0416.8+0105¹ Its inclusion in the 2FGL catalog is based on its detection in the 1-100 GeV
 41 band at a significance of 6.8σ ; the photon spectrum of the excess is well fit by a power law with a
 42 photon index of $1.96 \pm 0.16_{stat}$ and an integral flux in the 1-100 GeV band of $(6.9 \pm 1.4_{stat}) \times 10^{-10}$
 43 photons $\text{cm}^{-2} \text{s}^{-1}$.

44 1ES 0414+009 was among the 33 objects deemed to be very good candidates for TeV detections
 45 in the list of Costamante & Ghisellini (2002) and, as such, preliminary observations were taken by
 46 several TeV observatories with only upper limits resulting (Perez et al. 2003; Aharonian et al. 2004;
 47 Albert et al. 2008b). The HESS array of IACT telescopes detected the source in observations taken
 48 from 2005 to 2009 (Hoffman et al. 2009), with 224 excess events above 200 GeV in 73.7 hours of
 49 observation, corresponding to a statistically significant excess of 7.8σ (Abramowski et al. 2012).
 50 The HESS excess is well fit by a power law with a photon index of $3.5 \pm 0.3_{stat} \pm 0.2_{sys}$ and an
 51 integral flux above 200 GeV of $(1.9 \pm 0.2_{stat} \pm 0.4_{sys}) \times 10^{-12}$ photons $\text{cm}^{-2} \text{s}^{-1}$ or $\sim 0.6\%$ of the
 52 Crab Nebula flux in the same range.

53 2. VERITAS Observations

54 The VERITAS array (Ong et al. 2009) of IACTs located in southern Arizona (1.3 km m.a.s.l.,
 55 $31^\circ 40' 30'' \text{N}$, $110^\circ 57' 07'' \text{W}$) began 4-telescope array observations in September 2007 and is the most
 56 sensitive IACT for observations above 200 GeV currently in operation. The array is composed of
 57 four 12m diameter telescopes, each with a Davies-Cotton tessellated mirror structure of 345 12m
 58 focal length hexagonal mirror facets (total mirror area of 110 m^2). Each telescope focuses Cherenkov
 59 light from particle showers onto its 499-pixel PMT (photomultiplier tube) camera. Each pixel has
 60 a field of view of 0.15° , resulting in a camera field of view of 3.5° . VERITAS has the capability to
 61 detect and measure gamma rays in the 100 GeV to 30 TeV energy regime with an energy resolution
 62 of 15-20% and an angular resolution of $< 0.1^\circ$ on an event by event basis.

63 Between June and September 2009, VERITAS underwent a significant reconfiguration in which
 64 one of the four telescopes was moved to a new location making the geometric configuration of the
 65 array more symmetric and increasing the overall baseline (Perkins et al. 2009). This reconfiguration,
 66 as well as a marked improvement in the process for VERITAS mirror alignment (McCann et al.

¹.

67 2010), yielded a significant improvement in the VERITAS sensitivity at the level of 30%. In its
 68 current configuration, VERITAS can detect a 1% Crab Nebula flux at a 5σ significance in under 30
 69 hours, improved from the ~ 45 hours required with the previous array configuration and alignment.

70 The VERITAS observations of 1ES 0414+009 were made between January 2008 and February
 71 2011 and therefore comprise data taken in both array configurations. After quality selection cuts
 72 which remove data taken during poor weather and hardware conditions, approximately 25% (12.1
 73 hours) of the data for this analysis was taken with the original configuration and 75% (44.1 hours)
 74 were taken with the new configuration. The observations were made in “wobble” mode in which
 75 the source is offset from the center of the field-of-view of the cameras to maximize efficiency in
 76 obtaining both source and background measurements (Fomin et al. 1994). All data were processed
 77 and analyzed with the VERITAS Gamma-ray Analysis Suite (VEGAS, Cogan (2007)) with all results
 78 being successfully cross-checked by a second independent analysis package (Daniel 2008). The event
 79 selection criteria (cuts) used are based on the image morphology (*Mean Scaled Width* and *Length*),
 80 and the angular distance between the reconstructed position of the source in the camera plane
 81 and the *a priori* known source location (Aharonian et al. 1997) and were optimized on a simulated
 82 source with a soft energy spectrum ($\Gamma=4$) and a 7% Crab Nebula flux (at 200 GeV).

83 From the entire observational sample, a total of 822 events was detected in excess of the
 84 estimated background, corresponding to a statistical significance of 6.4σ (Li & Ma 1983). A two
 85 dimensional Gaussian fit to the VERITAS excess (VER J0416+011) is consistent with a point
 86 source located at $04^h16^m54^s \pm 5^s_{stat} \pm 6^s_{sys}$, $+1^\circ06'35'' \pm 1'47''_{stat} \pm 1'30''_{sys}$ (J2000), and with the
 87 optical AGN position (Hewitt & Burbidge 1993). VER J0416+011 is shown in Figure 1 along with
 88 the *Fermi*-LAT and optical positions.

89 The differential photon spectrum (see Figure 2) obtained from the VERITAS observations is
 90 well fit by a power law of the form $(1.6 \pm 0.3_{stat} \pm 0.8_{sys}) \times 10^{-11} \times (\frac{E}{0.3TeV})^{-3.4 \pm 0.5_{stat} \pm 0.3_{sys}} \text{cm}^{-2} \text{s}^{-1} \text{TeV}^{-1}$
 91 with a reduced chi-squared value ($\chi^2/\text{d.o.f}$) of 0.57 for 2 degrees of freedom. The VERITAS spectral
 92 parameters are consistent with those measured by HESS.

93 Due to its relatively low transit path on the sky for VERITAS, the data on 1ES 0414+009 were
 94 taken over a small range of zenith angles from 30° to 40° , resulting in an energy threshold ² of 200
 95 GeV. The integral flux, obtained from 1ES 0414+009 during VERITAS observations (derived from
 96 the spectral fit shown in Figure 2) was $(5.2 \pm 1.1_{stat} \pm 2.6_{sys}) \times 10^{-12} \text{photons cm}^{-2}$, or 2% of the Crab
 97 Nebula flux above 200 GeV. The construction of a lightcurve, binned on the timescale of VERITAS
 98 “dark runs” (intervals between full moons when skies are dark) shows no evidence for variability
 99 with a straight line fit yielding a reduced χ^2 of 0.55 for a chance probability of 88% (see Figure 3).
 100 The HESS observations, which indicated a 0.6% Crab Nebula flux, were made between October
 101 2005 and September 2009, overlapping only slightly with the VERITAS observations. While the

²The energy threshold is defined as the energy corresponding to the maximum of the product function of the observed spectrum with the collection area of the instrument.

102 VERITAS integral flux is larger than the HESS measurement, when statistical and systematic errors
 103 are taken into account (see Abramowski et al. (2012)), the two flux measurements are consistent
 104 with each other. However, given the current data we cannot rule out some long term variability in
 105 flux.

106 3. Multiwavelength Observations

107 3.1. *Fermi*-LAT

108 *Fermi*-LAT (Atwood et al. 2009) analysis was performed on all available photons from 0.3 to
 109 300 GeV accrued from the start of full *Fermi*-LAT science operations (August 4, 2008) until July 14,
 110 2011 (MJD 54682-55756), overlapping to a large degree with the VERITAS observations (January
 111 2008 - February 2011). The data were analyzed using the ScienceTools v9r23p1 package available
 112 from the Fermi Science Support Center (FSSC)³. Standard data quality cuts were applied as rec-
 113 ommended by the FSSC, with only “diffuse” class photons being used for this analysis (events with
 114 a high probability of being correctly identified as photons). An un-binned analysis was performed
 115 on all suitable photons coming from a region of radius 15° centered around 1ES 0414 +009 with
 116 all 2FGL sources (sources identified within the *Fermi*-LAT 2 year catalog) lying within 15° of 1ES
 117 0414+009 being modeled as well. In addition, both Galactic and extragalactic contributions to the
 118 diffuse background were modeled out using the P6_V11_Diffuse response functions. The *Fermi*-LAT
 119 systematic uncertainties are conservatively estimated at 10% for the energy range under evaluation
 120 in this work.⁴

121 The source is detected in the 0.3-300 GeV energy range with a test-statistic (TS) of 97 cor-
 122 responding to a detection significance of approximately 9.8σ. A lightcurve binned on a monthly
 123 timescale shows no evidence for variability in the *Fermi*-LAT energy range with a straight line
 124 fit yielding a reduced χ² of 0.81 for a chance probability of 76%(see Figure 3). The source spec-
 125 trum is well fit by a power law of the form $(6.3 \pm 1.5_{stat}) \times 10^{-13} (\frac{E}{1000 MeV})^{-1.9 \pm 0.1_{stat}}$ photons
 126 cm⁻²s⁻¹MeV⁻¹. For modeling purposes, spectral data points were obtained by dividing the data
 127 into five equally spaced bins in log(E) and requiring that each bin have a TS value of at least 4.
 128 These spectral points along with the associated fit to the *Fermi*-LAT data are shown in Figure
 129 2. As can be seen, the spectra from the two instruments (*Fermi*-LAT and VERITAS) connect
 130 to each other quite well, with the attenuating effect of the extragalactic background light on the
 131 observed TeV flux being readily apparent. It should be noted that the two spectra were taken over
 132 different (although overlapping), extended time periods and cannot be considered to constitute a
 133 simultaneous measurement of the GeV-TeV spectrum.

³<http://fermi.gsfc.nasa.gov/ssc/>

⁴http://fermi.gsfc.nasa.gov/ssc/data/analysis/LAT_caveats.html/

134 Using the ScienceTools function *gtprobsrc*, the excess seen in the *Fermi*-LAT data is consistent
 135 with a point source located at RA = $04^h16^m51^s \pm 8^s_{stat}$, DEC = $+1^\circ04'36'' \pm 2'2''_{stat}$ (J2000),
 136 consistent within errors with both the AGN position from Hewitt & Burbidge (1993) and the
 137 VERITAS source location (see Figure 1). It should be noted that all *Fermi*-LAT analysis results
 138 presented here are consistent with those derived for the source 2FGL J0416.8+0105 in the 2 year
 139 *Fermi*-LAT point source catalog.

140 3.2. *Swift*-XRT

141 Between 2006 and 2009, a total of 6.24 ks of *Swift*-XRT (Burrows et al. 2005) observations
 142 were taken on 1ES 0414+009 in “photon counting” (PC) mode. The reduced data products used
 143 for this study were downloaded from the UK *Swift* Science Center⁵ (Evans et al. 2009). Calibrated
 144 source and background files, along with the appropriate response files, were used as inputs to the
 145 spectral fitting package XSPEC v12.6 (Arnaud 1996). The spectrum between 0.3 and 10 keV was
 146 fit while allowing the neutral hydrogen (HI) column density to vary freely. The resulting HI column
 147 density was fit as $(1.7 \pm 0.16) \times 10^{21} \text{ cm}^{-2}$, higher than the value of $0.85 \times 10^{22} \text{ cm}^{-2}$ quoted in
 148 Kaberla et al. (2005). The spectrum is well fit (C-statistics were applied with less than 5% of model
 149 realizations providing a better fit) by a simple, absorbed power law (accounting for the redshift
 150 of the target) using the Wisconsin photoelectric cross sections (Morrison & McCammon 1983) or
 151 the “zwabs” model in XSPEC. The best fit for this model is provided by a normalization of $(6.1$
 152 $\pm 0.3) \times 10^{-3} \text{ ph cm}^{-2} \text{ s}^{-1}$ at 1 keV and a photon index of -2.4 ± 0.1 . All of these results are consistent
 153 with an analysis of the individual pointings analyzed separately, presented in Abramowski (2012).
 154 The deabsorbed source flux is measured as $(20.3 \pm 0.1) \times 10^{-12} \text{ erg cm}^{-2} \text{ s}^{-1}$ with no evidence for
 155 strong variability in the PC mode data presented here.

156 It should be noted, however, that ~ 2200 seconds of *Swift*-XRT observations taken in windowed
 157 timing (WT) mode on MJD 55231 and 55241 in 2010 indicate a large increase in the 0.3-10 keV flux
 158 from 1ES 0414+009. This data is fit by a simple, absorbed power-law with a derived photon index
 159 entirely consistent with the index from the PC mode observations, while showing a 0.3-10 keV flux
 160 of $58.8 (\pm 0.2) \times 10^{-12} \text{ erg cm}^{-2} \text{ s}^{-1}$, a factor of 2-3 higher than previous observations. Since the WT
 161 mode observations suggest a relatively short flaring episode, while the rest of the multi-wavelength
 162 data were taken over a much larger timescale, the WT mode observations are not included in the
 163 modeling effort in this work. However, we report these flare data as an indication of overall variable
 164 behavior in the system.

⁵<http://www.swift.ac.uk/>

165

3.3. MDM

166 1ES 0414+009 was observed at the 1.3m McGraw-Hill Observatory of the Michigan-Dartmouth-
 167 MIT (MDM) Observatory⁶ on the southwest ridge of Kitt Peak, during the nights of January 26 - 30,
 168 2011. Standard V, R, and I filters were used. The data were bias-subtracted and flat-field corrected
 169 using standard routines in IRAF, and comparative photometry was done based on comparison star
 170 magnitudes from (Fiorucci et al. 1998). For the construction of VRI SEDs, the magnitudes were
 171 corrected with the extinction coefficients $A_V = 0.39$, $A_R = 0.32$, and $A_I = 0.23$, as provided by the
 172 NASA/IPAC Extragalactic Database⁵ (NED). In addition to the MDM observations, we include
 173 archival U,B,V,R, and I filter data from Fiorucci et al. (2004) and Ulmer et al. (1983); along with
 174 infrared J, H, K values taken from Chen et al. (2005).

175

4. Multiwavelength SED and Modeling

176 The broadband SED constructed from the observations of 1ES 0414+009 is shown in Figure 4.
 177 Modeling of this SED proceeded by applying three distinct models of emission (two purely leptonic
 178 and one lepto-hadronic hybrid). The resulting predictions of the gamma-ray emission from these
 179 models were then modified to account for the attenuating effect of the extragalactic background
 180 light (EBL) using the Finke et al. (2010) EBL model.

181 The purely leptonic models employed to fit the SED are based on the premise that the high
 182 energy (GeV-TeV) emission is produced by inverse-Compton scattering of low energy ambient
 183 photons by a population of relativistic jet electrons (whose primary synchrotron emission makes
 184 up the lower energy X-ray peak). The variations between the models are based upon the nature
 185 of the photon field which is up-scattered: in synchrotron self-Compton (SSC) models, the target
 186 photon field is made of the original primary synchrotron photons (from the lower energy peak);
 187 while in external Compton (EC) models the emission includes the SSC contribution as well as
 188 inverse-Compton emission from a target photon field external to the jet.

189 The SSC model employed here is that of Böttcher & Chiang (2002) described also in detail
 190 in Acciari et al. (2009). In this model, the emission originates from a spherical distribution of
 191 relativistic electrons (of radius R) traveling along the jet axis with a Lorentz factor Γ , corresponding
 192 to a jet speed of $\beta_\Gamma c$. The jet viewing angle Θ_{obs} results in a Doppler boost factor given by $D =$
 193 $(\Gamma[1 - \beta_\Gamma \cos\Theta_{obs}])^{-1}$. In order to reduce the number of free parameters, we choose $\Theta_{obs} = 1/\Gamma$,
 194 leading to $\Gamma = D$.

195 In models such as these, particles are injected with some distribution in energy and are sub-
 196 sequently cooled (i.e. lose energy by radiative mechanisms) or escape the accelerating region and

⁶<http://mdm.kpno.noao.edu/>

⁵<http://ned.ipac.caltech.edu/>

197 no longer contribute to emission. The models under consideration here result in an equilibrium
 198 between these factors (i.e. acceleration and cooling/escape). Here we parameterize the front end
 199 of the model by injecting electrons into the spherical region with a power-law distribution given by
 200 $Q(\gamma) = Q_0\gamma^{-q_e}$ bounded by the cutoff parameters $\gamma_{emin}, \gamma_{emax}$. The escape time in the model is
 201 parameterized by η which corresponds to an escape time t_{esc} of the particles of $t_{esc} = \eta R/c$. The
 202 resulting equilibrium particle distribution in the emission volume corresponds to a kinetic power
 203 L_e in relativistic electrons. The synchrotron emission is determined by a tangled magnetic field B ,
 204 corresponding to a power L_B in Poynting flux. Furthermore, the equipartition parameter $\epsilon_{eB} =$
 205 L_B/L_e is evaluated during the modeling process to give an evaluation of how reasonable the model
 206 is physically; it is reasonable to expect that most models that fit HBL emission well would generate
 207 values for ϵ_{eB} within the range of $\sim 0.1-1.0$.

208 The EC model used in this analysis incorporates all the above SSC model attributes while
 209 adding an additional emission component due to inverse-Compton scattering off an external photon
 210 source (corresponding to a standing perturbation of the jet flow). Hence its modeling parameters
 211 are identical to the SSC parameters along with the addition of the blackbody temperature and
 212 energy density of the external photon field (T_{EC}, u_{EC}).

213 In contrast to the two leptonic models above, the lepto-hadronic model used for this analysis
 214 assumes that the high energy emission is dominated by proton synchrotron and pion decay emission
 215 processes. An additional model component is generated from the electromagnetic cascades from
 216 $\gamma - \gamma$ absorption between multi-TeV photons (from charged-pion decay products) and low-energy
 217 synchrotron photons from ultrarelativistic leptons. Similarly to the SSC and EC models, the
 218 protons are injected with a power-law spectrum (parameterized by $n(\gamma) = \gamma^{-q_p}$ bracketed by the
 219 lower and higher energy cutoffs $\gamma_{pmin}, \gamma_{pmax}$) corresponding to a kinetic power L_p in relativistic
 220 protons, which we compare with the power L_e in relativistic primary leptons and the Poynting flux
 221 power L_B . All parameter values described here, as well as resulting equipartition values, are listed
 222 in Table 1.

223 As can be seen in Figure 4, while both leptonic models fit the TeV spectrum reasonably well,
 224 neither provides a satisfactory fit to the observed broad GeV peak (in contrast to the relatively
 225 sharp synchrotron peak). The extremely wide separation between the synchrotron and gamma-ray
 226 peak implies a very large γ of the electrons (see Table 1), which then implies a very low B-field
 227 in order to achieve the observed synchrotron peak. A large Doppler factor ($D = 40$) can then
 228 help reduce the overall power requirements in the electrons to maintain values close to reasonable
 229 equipartition conditions.

230 We find that the lepto-hadronic model provides a more satisfactory fit to the observed SED.
 231 The primary proton synchrotron emission matches the GeV - TeV emission very well, while the
 232 lower end of the GeV spectrum is reproduced by emission from electromagnetic cascades. It is
 233 clear however, that this model still over/underpredicts some of the *Fermi*-LAT GeV points and is
 234 far from equipartition. It is possible that additional components may be required in this model to

235 more accurately describe the system. Additionally, the model predicts a relatively strong flux in
 236 the very hard X-ray/soft gamma-ray regime; an energy range which is completely unexamined by
 237 the observations described in this work.

238 5. Summary

239 The VERITAS array of telescopes has detected the distant blazar 1ES0414+009 in 56.2 hours
 240 of observations, resulting in a detection at a statistical significance of 6.4σ . The differential photon
 241 spectrum from the source is well fit by a power law with normalization and photon index parameters
 242 given by $(1.6 \pm 0.3_{stat} \pm 0.8_{sys}) \times 10^{-11} \times \frac{E}{0.3 \text{ TeV}}^{-3.4 \pm 0.5_{stat} \pm 0.3_{sys}} \text{ cm}^{-2} \text{ s}^{-1} \text{ TeV}^{-1}$. The integral flux
 243 from the source is measured as approximately 2% of the Crab Nebula flux above 200 GeV. While
 244 this is a larger integral flux than the HESS measurement (0.6% Crab above 200 GeV), when
 245 statistical and systematic errors are taken into account (see Abramowski et al. (2012)), the two
 246 flux measurements are consistent with each other.

247 We have also presented multiwavelength data on 1 ES 0414+009 from *Fermi*-LAT, *Swift*-XRT,
 248 and the MDM observatory. We combine these data with archival optical data to construct a
 249 broadband SED which shows a very narrow synchrotron peak in contrast to the relatively broad
 250 GeV-TeV gamma-ray peak. The SED is not well fit by homogenous leptonic one-zone models,
 251 however a hybrid lepto-hadronic model provides a reasonable fit to the observed data in a strongly
 252 magnetically dominated jet.

253 Although the lepto-hadronic model provides a better fit to the observed SED, it still does not
 254 accurately predict the apparently complicated form of the GeV-TeV emission. It should be noted,
 255 however, that both the GeV and TeV spectral data points have relatively large error bars and do
 256 not take systematic errors into account. Therefore, it is difficult to accurately constrain or improve
 257 any SED models until much more precise measurements of the GeV-TeV regime emission are made.

258 The study of sources at such a relatively high redshift can shed light on more fundamental sci-
 259 ence topics such as the characteristics of the extragalactic background light (EBL) and intergalactic
 260 magnetic fields (IGMF). While we do not make any statements about these topics in this current
 261 work, as the catalog of high redshift TeV detections increases (with an accompanying increase in
 262 statistics on individual sources) our understanding of the properties of the EBL and IGMF will
 263 increase as well. A subsequent study of this source with these goals in mind will be the subject of
 264 a future publication. Additionally, the next generation IACT array CTA (Actis et al. 2011) (along
 265 with additional data collection with *Fermi*-LAT to improve the MeV-GeV spectral measurement)
 266 will be able to much more precisely measure the high energy emission of distant objects such as
 267 1ES 0414+009, providing valuable insights into the nature of some of the most distant TeV targets
 268 known as well as fundamental measurements of the EBL and IGMF.

6. Acknowledgements

269

270 This research is supported by grants from the U.S. Department of Energy Office of Science,
271 the U.S. National Science Foundation and the Smithsonian Institution, by NSERC in Canada, by
272 Science Foundation Ireland (SFI 10/RFP/AST2748) and by STFC in the U.K. We acknowledge
273 the excellent work of the technical support staff at the Fred Lawrence Whipple Observatory and at
274 the collaborating institutions in the construction and operation of the instrument. This work also
275 made use of data supplied by the UK *Swift* Science Data Centre at the University of Leicester.

REFERENCES

276

- 277 Abramowski, A., et al. 2012, *A&A*, 538, A103
- 278 Acciari, V., et al. 2009, *ApJ*, 707, 612
- 279 Actis, M., et al. 2011, *Exp. Astron.* 32, 193
- 280 Aharonian, F., et al. 1997, *Astro. Part. Phys*, 6, 343
- 281 —. 2004, *A&A*, 419, 25
- 282 Albert, J., et al. 2008a, *Science*, 320, 1752
- 283 —. 2008b, *ApJ*, 681, 944
- 284 Arnaud, K. 1996, *Astronomical Data Analysis Software and Systems V*, eds. G. Jacoby, and J.
285 Barnes, *ASP Conf. Series*, 101, 17
- 286 Atwood, W., et al. 2009, *ApJ*, 697, 1071
- 287 Beckmann, V., et al. 2002, *A&A*, 383, 410
- 288 Böttcher, M., & Chiang, J. 2002, *ApJ*, 581, 127
- 289 Burrows, D., et al. 2005, *Space Science Reviews*, 120, 165
- 290 Chen, P., Fu, H., & Gao, Y. 2005, *New Astronomy*, 11, 27C
- 291 Cogan, P. 2007, In *Proceedings of the 31st ICRC*, Merida, MX, astro-ph/0709.4233
- 292 Costamante, L., & Ghisellini, G. 2002, *A&A*, 384, 56C
- 293 Daniel, M. 2008, in *Proc. 30th Int. Cosmic Ray Conf.*, Vol. 3, 1325
- 294 Evans, P., et al. 2009, *MNRAS*, 397, 1177
- 295 Finke, J., Razzaque, S., & Dermer, C. 2010, *ApJ*, 712, 238

- 296 Fiorucci, M., Ciprini, S., & Tosti, G. 2004, *A&A*, 419, 25F
297 Fiorucci, M., Tosti, G., & Rizzi, N. 1998, *PASP*, 110, 105
298 Fomin, V., et al. 1994, *Astro. Part. Phys*, 2, 137
299 Halpern, J., et al. 1991, *Astron. Journal*, 101, 818
300 Hewitt, A., & Burbidge, G. 1993, *ApJ.Suppl.*, 87, 451H
301 Hoffman, W., et al. 2009, *ATEL* 2293
302 Horan, D., et al. 2002, *ApJ*, 571:753-762
303 Kaberla, P., et al. 2005, *A&A*, 440, 775
304 Li, T., & Ma, Y. 1983, *ApJ*, 272, 317
305 McCann, A., Hanna, D., Kildea, J., & McCutcheon, M. 2010, *Astropart.Phys.*, 32,6, 322
306 Morrison, R., & McCammon, D. 1983, *ApJ*, 270, 119
307 Ong, R., et al. 2009, in in proceedings of 31st ICRC, Lodz, Poland, astro-ph/912.5355
308 Perez, I. D. L. C., et al. 2003, *ApJ*, 599, 909
309 Perkins, J., et al. 2009, in in the proceedings of the 2009 Fermi Symposium, eConf Proceedings
310 C091122
311 Ulmer, M., et al. 1983, *ApJ*, 270, L1
312 Ulmer, M. P., et al. 1980, *ApJ*, 235, 531
313 Wolter, A., et al. 1998, *A&A*, 335, 889

Parameter	SSC	EC	Lepto-Hadronic
γ_{emin}	2×10^5	9×10^4	4.8×10^3
γ_{emax}	5×10^6	3×10^6	1.0×10^5
q_e	3.5	3.5	3.6
γ_{pmin}	-	-	1.0×10^3
γ_{pmax}	-	-	1.0×10^{11}
q_p	-	-	1.8
η	120	40.0	3
B (G)	0.008	0.044	30
Γ	40	40	20
R (cm)	2.1×10^{17}	7×10^{16}	1.0×10^{16}
$\Theta_{obs}(\circ)$	1.43	1.43	2.86
$\Delta t_{min.variability}(hrs)$	62.5	20.9	5.95
$T_{EC}(K)$	-	1000	-
$u_{EC}(erg/cm^{-3})$	-	3×10^{-9}	-
L_e (erg/s)	3.07×10^{44}	6.93×10^{43}	1.91×10^{41}
L_B (erg/s)	1.69×10^{43}	5.69×10^{43}	1.35×10^{47}
ϵ	0.055	0.82	7.06×10^5
L_p	-	-	8.0×10^{43}
$\epsilon_{pB}=L_B/L_p$	-	-	1.6×10^3
$\epsilon_{pe}=L_e/L_p$	-	-	2.4×10^{-3}

Table 1: Summary of the emission zone parameters used for modeling the synchrotron self-Compton, external Compton, and lepto-hadronic models as described in the text.

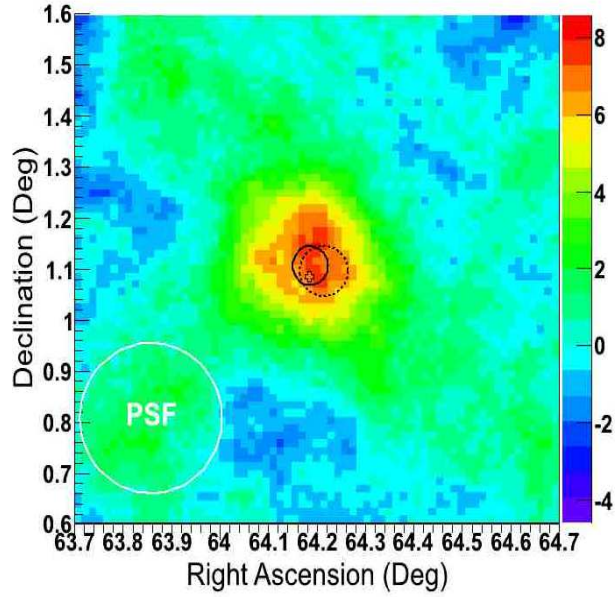


Fig. 1.— The two-dimensional significance map of the 1ES 0414+009 region from VERITAS observations made at VHE gamma-ray energies with the color scale representing units of standard deviation of the corresponding excess. The cross represents the optical position of the AGN from Hewitt & Burbidge (1993), the solid circle represents the best fit VERITAS position with associated statistical and systematic errors, and the dotted circle represents the position of the excess observed by *Fermi*-LAT (statistical error only). The white circle in the lower left corner represents the scale of the VERITAS point spread function of 0.12° .

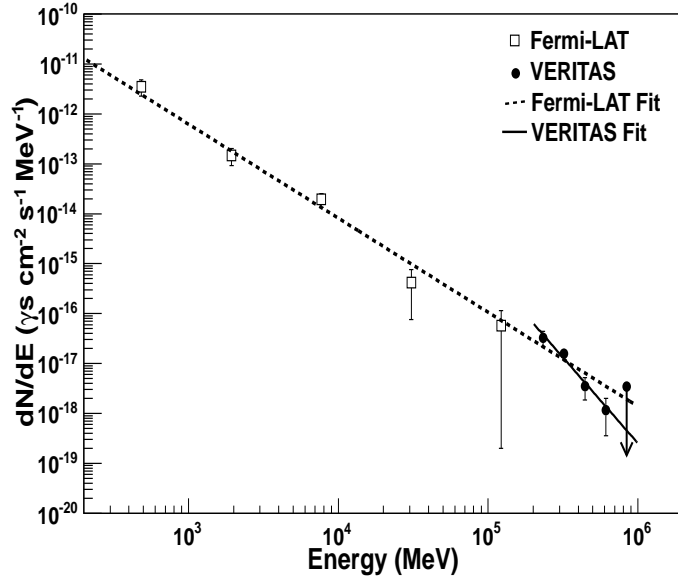


Fig. 2.— The derived spectral points from both *Fermi*-LAT and VERITAS observations (non-simultaneous) of 1ES 0414+009. The dotted line shows the power law fit to the *Fermi*-LAT spectrum extrapolated to TeV energies, while the solid line shows the power-law fit to the observed VERITAS TeV spectrum.

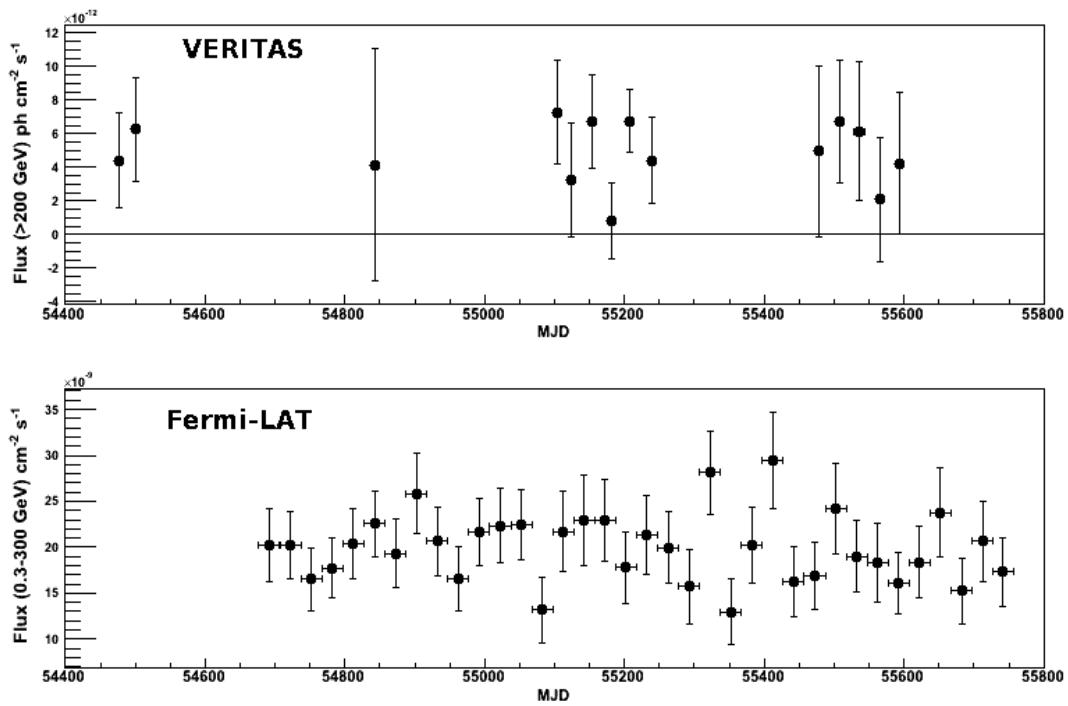


Fig. 3.— The VERITAS (top) and *Fermi*-LAT light curves for the observations detailed in this work. Errors shown on both light curves are statistical only.

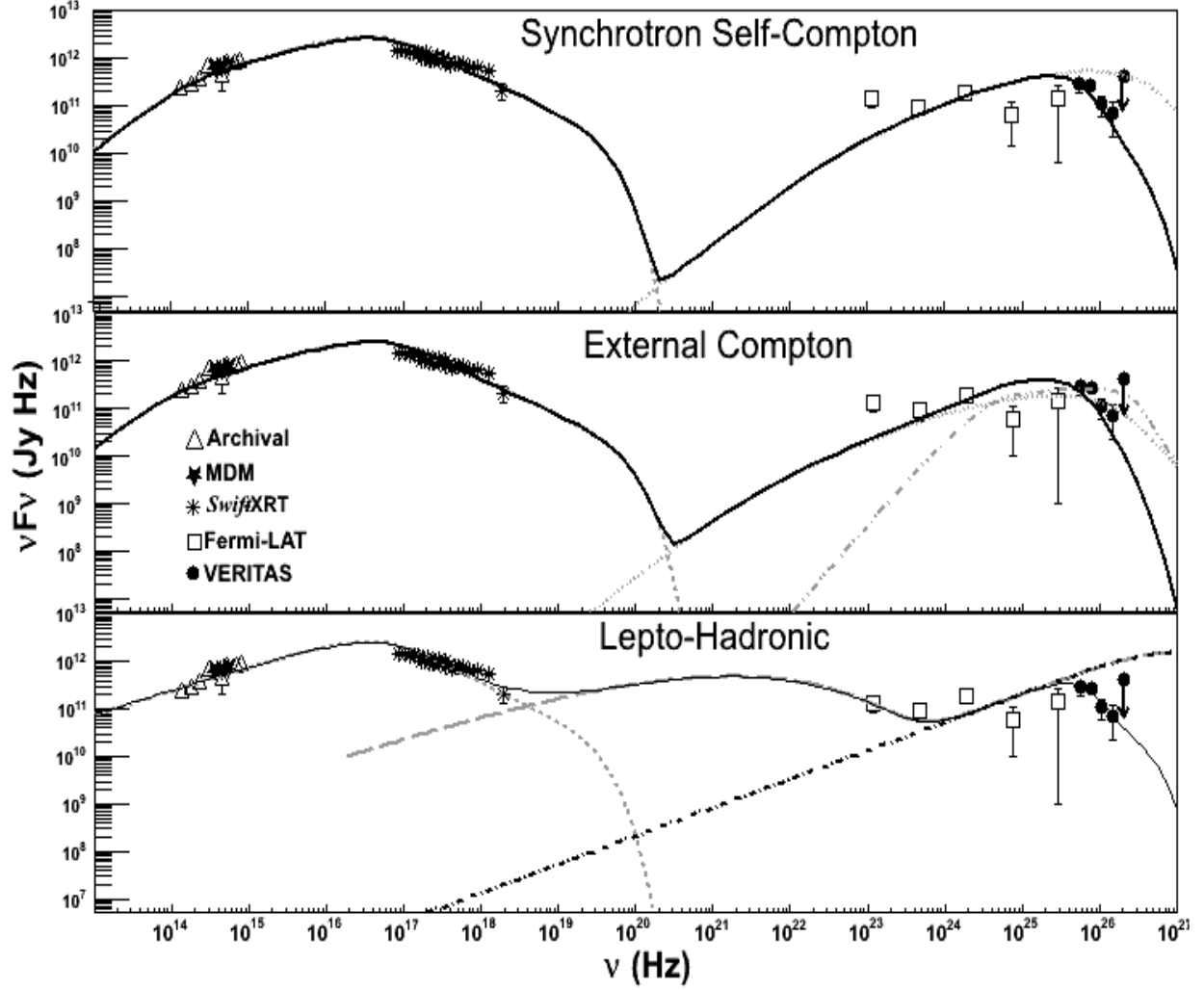


Fig. 4.— The broadband SED constructed from the data sets described in the text. The top panel shows the SSC model results with contributions from primary synchrotron (dashed line), synchrotron self-Compton (dotted line), and EBL correct total (solid line). The middle panel shows the external Compton model results with contributions from primary synchrotron (dashed line), synchrotron self-Compton (dotted line), external Compton (dotted-dashed line), and EBL corrected total (solid line). The bottom panels shows the lepto-hadronic results with contributions from electron synchrotron (dotted line), proton synchrotron (dotted-dashed), proton synchrotron with electromagnetic cascades (dashed line), and EBL corrected total.